# Constraints and Opportunities for Detecting Land Surface Phenology in Drylands

Shawn D. Taylor[1,2*], Dawn M. Browning[1], Ruben A. Baca[1], and Feng Gao[3]

[1]US Department of Agriculture, Agricultural Research Service, Jornada Experimental Range, New Mexico State University, Las Cruces, New Mexico, 88003, USA

[2]Oak Ridge Institute for Science and Education (ORISE), Oak Ridge, Tennessee, 37830, USA

[3]US Department of Agriculture, Agricultural Research Service, Hydrology and Remote Sensing Laboratory, Beltsville, Maryland, 20705, USA

[*]Corresponding author. Email: shawn.taylor@usda.gov

**Abstract**

Land surface phenology, the tracking of seasonal productivity via satellite remote sensing, enables global scale tracking of ecosystem processes, but its utility is limited in some areas. In dryland ecosystems low vegetation cover can cause the growing season vegetation index (VI) to be indistinguishable from the dormant season VI, making phenology extraction impossible. Here, using simulated data and multi-temporal UAV imagery of a desert shrubland, we explore the feasibility of detecting LSP with respect to fractional vegetation cover, plant functional types, and VI uncertainty. We found that plants with distinct VI signals, such as deciduous shrubs with a high leaf area index, require at least 30-40% fractional cover on the landscape to consistently detect pixel level phenology with satellite remote sensing. Evergreen plants, which have lower VI amplitude between dormant and growing seasons, require considerably higher cover and can have undetectable phenology even with 100% vegetation cover. We also found that even with adequate cover, biases in phenological metrics can still exceed 20 days, and can never be 100% accurate due to VI uncertainty from shadows, sensor view angle, and atmospheric interference. Many dryland areas do not have detectable LSP with the current suite of satellite based sensors. Our results showed the feasibility of dryland LSP studies using high-resolution UAV imagery, and highlighted important scale effects due to within canopy VI variation. Future sensors with sub-meter resolution will allow for identification of individual plants and are the best path forward for studying large scale phenological trends in drylands.

# 1 Introduction

Landscape patterns in seasonal productivity [hereafter 'land surface phenology' (LSP)] enable ecosystem scale tracking of the drivers and consequences of a changing climate. Satellite sensor-derived vegetation indices (VIs) track the progression of green vegetation throughout the year, and from this time series the seasonal transitions between the dormant and growing seasons are derived [1–8]. Numerous studies measure the short- and long-term LSP trends, linking them to drivers such as weather and climate, land cover change, and disturbances [9]. Yet the use of LSP is limited outside regions with adequate vegetation cover and plants with distinct seasonal change. Temperate deciduous forests have the most distinct LSP signal, while in other vegetation types LSP is difficult to discern due to combinations of low signal-to-noise ratio between growing and dormant season VI, high snow cover, and low vegetation cover [10, 11].

In dryland ecosystems low vegetation cover is the primary limitation in detecting land surface phenology [12]. High soil fractional cover can cause the growing season VI to be indistinguishable from the dormant season VI, making phenology extraction impossible. Additionally, some areas with adequate vegetation cover are dominated by evergreen vegetation, thus can have a growing season VI too low to reliably detect seasonal transitions [13]. Even in areas with high vegetation cover and plants with distinct signals, phenology may be impossible to detect some years due little to no plant productivity from inadequate precipitation. These limitations cause drylands to be excluded in many large scale LSP analyses [14–18] Most studies focusing on drylands evaluate aggregate or peak annual VI as opposed to distinct seasonal transitions [13, 19], and even then can occasionally have inconclusive results [20, 21].

Here we explore key attributes of VI time series and how they affect reliable detection of LSP in dryland ecosystems. We use a spectral mixing model to simulate LSP with varying ranges of plant fractional cover, seasonal VI amplitude, and VI uncertainty to determine the feasibility of detecting LSP in different scenarios. We then use high spatial resolution, multi-temporal unmanned aerial vehicle (UAV) imagery to verify some of these relationships. Finally we discuss the feasibility of detecting dryland LSP currently and in the future.

# 2 Methods

## 2.1 Model Simulation

First we describe a conceptual model of an annual dryland VI time series and how it translates into phenology. Using spectral mixing, and assuming a linear aggregation, the VI at a pixel scale for a single date can be decomposed into the following parts:

$$VI_{Pixel} = Cover_{veg} \times VI_{veg} + (1 - Cover_{veg}) \times VI_{soil} + \varepsilon \tag{1}$$

Where $Cover_{veg}$ is the fractional vegetation cover within the pixel, $VI_{veg}$ and $VI_{soil}$ are the average VI values of the endmembers of all plants and soil, respectively, and $\varepsilon$ is the error term from uncertainty in sensor view angle, shadows, and atmospheric interference [22, 23]. Extraction

of phenological metrics relies on the $VI_{pixel}$ being distinctly higher in the growing season than the dormant season.

Here we explore how variation in the three components in Eq. 1 (i.e., ranges of plant fractional cover, seasonal VI amplitude, and VI uncertainty) affect the ability to detect a distinct phenological signal in sparsely vegetated areas. We start with an idealized annual VI curve derived from a double sigmoid model to represent the VI of single plant canopy (Figure 1, [24]). The curve's amplitude (i.e., the difference between dormant and peak VI values) reflects a combination of plant functional type and leaf area index (LAI). The seasonal amplitude of non-evergreen plants is driven by LAI up to an LAI of approximately 2, while evergreen plants have little to no seasonal amplitude [25, 26]. Higher LAI will generally lead to higher amplitudes, with this effect being more prominent in deciduous plants than evergreen plants [27, 28]. The leaves of senesced grasses have distinctly lower NDVI than green leaves, thus are expected to behave similarly to deciduous plants [29].

Using the curve values at 8-day intervals for a full calendar year, we apply Eq. 1 with fractional vegetation values of 60% and 30%, then include gaussian noise with a mean of 0 and standard deviation (SD) of 0.02 to represent $\varepsilon$, resulting in an 8-day VI time series for a full calendar year (Figure 1B, 1C points). A cubic smoothing spline is then fit to the 8-day $VI_{pixel}$ values and phenology metrics extracted using a threshold of 10% of the relative maximum value. Figure 1 shows how the phenological metrics change due solely to differences in fractional vegetation cover, even though the underlying plant phenology, $VI_{veg}$, is the same. In this example there is still adequate amplitude to detect transitions, but at a low enough fractional vegetation cover the $VI_{pixel}$ amplitude will be too low to detect transition dates.

For the simulation analysis we repeated this process while varying the three different factors from Eq. 1: 1) the fractional vegetation cover ($Cover_{veg}$), using values from 0-100%, 2) the amplitude of $VI_{veg}$ from dormant to peak, adjusted using a parameter in the double sigmoid model, and 3) the size of the error term $\varepsilon$ using values of 0.01 and 0.04 for the standard deviation of the gaussian noise. For each combination we repeated the process 100 times. A low growing season VI relative to the dormant season is one of the main challenges in dryland LSP [28]. Phenological extraction methods account for this in several ways. A common approach is discarding pixels which do not exceed a threshold of 0.1 VI units between the dormant season and peak growth (i.e., a minimum $VI_{pixel}$ amplitude of 0.1; [6, 11, 14, 18]), while others have used statistical power methods of the time-series to filter out pixels with low signal-to-noise [30]. Here we evaluate the detectability of LSP in two ways: 1) The frequency at which the $VI_{pixel}$ meets or exceeds an amplitude of 0.1 VI units, and 2) mean absolute error (MAE) in the estimated phenological metrics start of season (SOS), end of season (SOS), and peak.

## 2.2 UAV Study Area

We verified the effect of fractional vegetation cover on LSP detection by evaluating LSP of a deciduous shrubland and in situ observations of canopy greenness. We acquired UAV imagery for a long-term study site (NORT) on the Jornada Experimental Range (JER) for eight dates in 2019. The JER is located in the Chihuahuan Desert near Las Cruces, New Mexico, U.S., and is a low-

diversity, mixed perennial grassland and evergreen/deciduous shrubland that receives on average 254-mm rain annually with 50% falling between July and October [31]. The site is ideal for testing patterns of LSP detectability and accuracy since it has low to moderate fractional vegetation cover consisting primarily of a single plant species.

The NORT site consists of mostly sandy soil and has approximately 30% cover of honey mesquite (*Prosopis glandulosa*) with occasional four-wing saltbush (*Atriplex canescens*) shrubs growing in some mesquite patches and snakeweed (*Gutierrezia sarothrae*) in the interpatch areas. In addition to UAV imagery we also collected weekly in situ observations of mesquite canopy greenness following USA-National Phenology Network intensity protocols (Denny et al. 2014). Each week during 2019, for five focal mesquite shrubs, we estimated the percentage of green leaves within each individual shrub canopy in seven bins (0%, 1-4%, 5-24%, 25-49%, 50-74%, 74-94%, 95-100%).

## 2.3 UAV Acquisition and Processing

To collect aerial imagery we deployed a 3DR SOLO UAV equipped with a Micasense RedEdge camera (https://micasense.com/) and Downwelling Light Sensor (DLS) at an altitude of approximately 28 meters above ground level resulting in a ground sampling distance (GSD) of 1.8 cm. The total image extent was 2.1 ha. Aerial surveys were conducted on eight days in 2019 (April 2, April 25, July 5, August 14, September 26, October 16, November 13, December 20) to characterize mesquite phenology. Flights were planned using Mission Planner software, conducted at mid-day (between 10 a.m. and 12 p.m.); given an east-west corridor pattern, forward lap of 85% and side lap of 75% ensured sufficient pixel overlap between adjacent images for proper alignment and mosaicking. Images of a 6" x 6" Micasense Calibrated Reflectance Panel were taken before each flight for radiometric calibration. We use fixed ground control points within the image footprint as the basis for the geometric correction; ground control points were previously surveyed using a Trimble Geo 7X handheld Global Positioning System. Ortho-mosaics of drone imagery were created using Pix4D software (version 4.2.27, https://www.pix4d.com/) using the following steps:

1. Initial processing: Keypoints Image Scale, full; Matching Image pairs, Aerial Grid or Corridor; Matching Strategy, Use Geometrically Verified Matching; targeted Number of Keypoints, Automatic; Calibration, Alternative; Rematch, Automatic.

2. Point Cloud and Mesh: N/A

3. DSM, Orthomosaic and Index: Resolution, Automatic; DSM Filters, Use Noise Filtering, Use Surface Smoothing (Sharp); Orthomosaic, GeoTIFF; Radiometric Processing and Calibration, Camera and Sun Irradiance; Resolution, Automatic; Downsampling Method, Gaussian Average; Reflectance Map, GeoTIFF, Merge Tiles.

After initial alignment, GCPs in aerial imagery were manually selected and geolocation tags re-registered with previously surveyed, sub-centimeter geolocation information acquired with the Trimble GPS. The project is then re-optimized with the new geolocation information for more accurate results with RMSE errors ranging from 0.10 to 0.02 meters.

To compute the reflectance value of each pixel, Radiometric Processing and Calibration correction type was set for Camera and Sun Irradiance in orthomosaic and radiometric correction step 3 above. This function in Pix4D calibrates images using irradiance and sun angle measurements obtained from the DLS and the calibration reflectance panel [32]. Reflectance values were used to calculate the normalized difference vegetation index (NDVI) images for the study site for each image date.

Using this time series of NDVI rasters we developed a sampling routine to test the detectability of phenology with respect to fractional vegetation cover similar to the simulation study. We randomly placed 12,000 simulated pixels across the site with sizes of 2, 4, 6, 8, or 16 meters. We then extracted the average NDVI within each one for each image date. This random placement allowed us to produce 12,000 annual NDVI time series representing a range of fractional cover for honey mesquite across several pixel resolutions. The average shrub diameter is approximately 8m, so multiple pixel sizes allow us to test both L- and H-resolution LSP detection [33]. As in the simulation study, each annual time series was fit with a cubic smoothing spline and we then calculated whether the smoothed time series exceeded a 0.1 NDVI threshold and extracted phenology metrics using a 10% of relative max threshold method and the curvature method as described below.

To determine the fractional vegetation cover within each simulated pixel we developed a map of shrub canopy cover for the site using hand annotation of an RGB image, resulting in a raster at the same extent and resolution of the NDVI imagery where each pixel is classified as either mesquite canopy or soil (Figure S1). Fractional vegetation cover was then calculated as the proportion of mesquite pixels within each simulated 2-16m pixel. To calculate the MAE of the UAV imagery-derived phenology estimates, we used the weekly in-situ observations of mesquite canopy greenness at the site as described above. We fit a single cubic smoothing spline using observations from all five individuals with the midpoint of each percent canopy cover bin. From the spline we calculated the DOY for SOS and EOS using the two methods described below.

## 2.4 Detection Methods and Analysis

Many remote sensing algorithms have been developed in recent decades for estimating transition dates from VI timeseries. They can be categorized in the threshold, curvature, trend, and priori curve-based approach [34]. The threshold-based approach uses the predefined threshold of amplitude of VI (difference between base and maximum VI) to detect SOS, EOS, and other phenological metrics [3, 6, 7]. The curvature-based approach detects the inflection points that show the quickest changes in the VI time series [1, 5, 35]. The trend-based estimate transitions from changing trends in the VI time series and are mainly used for near real-time crop monitoring [36, 37]. The priori curve-based approaches combine the reference curve from previous years and current observations to map LSP for the current year [4, 38, 39]. In this paper, we use two approaches to evaluate LSP dynamics in drylands: a threshold and curvature model. The threshold-based approach is an established methodology, is simple to implement, and has been used to produce LSP data products from the Advanced Very High Resolution Radiometer (AVHRR), Moderate Resolution Imaging Spectroradiometer (MODIS), and the Harmonized Landsat and Sentinel-2 (HLS) data [3, 6, 7]. The curvature-based approach does not depend on a-prior thresholds and can capture transition dates

with relatively small changes in the VI timeseries, and has been used to produce Collection 5 MODIS phenology and VIIRS phenology [1, 35].

For the threshold method SOS (EOS) was estimated as the DOY when the smoothed VI curve exceeded (fell below) a 10% threshold of the relative maximum VI value. For the curvature method SOS (EOS) was estimated as the DOY when the smoothed VI curve had the highest (lowest) rate of change. The peak estimate was the day of year (DOY) of the maximum smoothed VI value, thus was independent of the SOS/EOS method. For the MAE of the in simulated study the true metrics are derived using the respective method of the original $VI_{veg}$ annual curve. Since we are using a simulated VI it can be interpreted as either EVI or NDVI. Peak was the DOY of maximum canopy greenness. All code for this analysis is available in the Zenodo data repository (https://doi.org/10.5281/zenodo.4777207).

# 3 Results

## 3.1 Model Simulation

When the fractional vegetation cover is 10% or less the $VI_{pixel}$ curve rarely exceeds the 0.1 threshold between the dormant and peak growing seasons (Figure 2). Even an extremely "bright" plant with a $VI_{veg}$ amplitude of 0.8 will meet the 0.1 threshold less than half the time. At 60% fractional vegetation cover plants with $VI_{veg}$ amplitude of 0.2 or higher consistently exceed the needed threshold. Plants with a $VI_{veg}$ amplitude of 0.1, which might be seen in some evergreen species, never consistently exceed the 0.1 $VI_{pixel}$ threshold even with nearly 100% fractional cover.

Increasing the uncertainty dampened the effect of increasing fractional vegetation cover. When the uncertainty SD was 0.04, and combined with low fractional vegetation cover, a larger proportion of simulation runs exceeded the $VI_{pixel}$ 0.1 threshold, with the reverse happening at higher fractional vegetation cover (Figure 2). Thus, VI uncertainty propagates into uncertainty in detecting dryland LSP. For example a pixel with low vegetation cover may, in some years, have seemingly detectable LSP due solely to chance instead of significantly higher productivity.

Even with a phenological pattern that is consistently detectable, the combined effects of soil background, VI uncertainty, and methodology still cause some level of bias in the estimated phenological metrics. For example, given a plant with an $VI_{veg}$ amplitude of 0.2 and 60% fractional cover, all phenological metrics had mean average error (MAE) of at least 10 (and up to 50) days in our simulations using a 10% of maximum threshold (Figure 3). The MAE of estimates improved with increasing vegetation cover, with increasing $VI_{veg}$ amplitude, and from using the curvature instead of threshold-based method for SOS and EOS estimation. The highest errors were seen with low $VI_{veg}$ amplitude and high (0.04) VI uncertainty. Peak greenness was more accurate than SOS or EOS in most instances when using a threshold method, especially when the $VI_{veg}$ amplitude was low (0.4 or 0.1). The curvature method outperformed the threshold method in all instances except one, when estimating EOS with a $VI_{veg}$ amplitude of 0.1. The curvature method was particularly accurate in estimating SOS of this simulated data, especially when fractional vegetation cover was low. Increasing the VI uncertainty from 0.01 to 0.04 increased the MAE of estimates in all cases

regardless of fractional cover, $VI_{veg}$ amplitude, or methodology.

### 3.2 UAV Imagery

Annual mesquite NDVI exceeded a 0.1 minimum amplitude consistently when fractional vegetation cover was between 25% and 60%, depending on the simulated pixel size (Figure 4). The discrepancy with pixel size is similar to what is seen with increasing VI uncertainty in the simulation analysis, but here reflects the high variation in NDVI within the mesquite canopy (Figure S2, S3). For example, given a single mesquite shrub 8m in diameter, 2m pixels randomly located within the canopy can have a wide range of NDVI values for a single acquisition date, resulting in varying amplitude given the same fractional cover. Larger pixel sizes essentially have larger samples to better estimate the mean NDVI of canopies. This leads to a scale dependence for LSP detectability at these extremely fine-scale spatial resolutions. At the 16m pixel size the NDVI variation is reduced enough to result in a relationship between fractional vegetation cover and LSP detectability which most reflects our simulated results.

As in the simulation study, errors of LSP derived transition dates decreased with increasing vegetation cover for all metrics (Figure 5). Because of the scale effect from canopy variation in NDVI, smaller pixel sizes had large variation in error rates for any given fractional cover. Using pixel sizes of 8 or 16m the MAE stabilized at approximately 20% mesquite cover for SOS and EOS using the threshold method. The curvature method produced slightly more accurate estimates when mesquite fractional cover was less than 20%, but equivalent or less accurate estimates at high mesquite cover. The MAE for peak estimates, which was independent to the threshold or curvature methods, was never below 40 days and commonly greater than 60. This suggests a dissimilarity between peak greenness from UAV imagery versus in-situ observations.

## 4 Discussion

With simulated VI curves we showed the limitations in detectability of dryland LSP with respect to fractional vegetation cover, VI amplitude, and VI uncertainty. The required fractional vegetation cover to detect phenology depends on the underlying plant traits, with evergreen plants needing higher cover than non-evergreen plants. Even when the seasonal amplitude of a pixel exceeds a minimum QA threshold, phenological metrics of sparsely vegetated drylands can still have considerable error due to other factors. We used UAV imagery of a deciduous shrubland to validate these results, and also highlighted how within canopy VI variation affects LSP detection in high resolution imagery. The algorithm used for transition date estimation affected results as well, with the curvature method outperforming the threshold method with simulated data, and the threshold method having better or equivalent results than the curvature method with UAV imagery time series.

The three primary factors affecting LSP detection and accuracy vary across ecosystems, sensors, and with plant community composition. They also interact such that the detectability is not uniform across vegetation types with similar characteristics. For example 40% fractional cover may be adequate to detect LSP in a deciduous shrubland, but likely not in an evergreen shrubland. Neither

may have detectable LSP with some satellite sensors due to higher VI uncertainty. The methodology and algorithms used can also affect results, and some methods may be more suitable depending on the underlying time series characteristics. Here we explore these factors in detail, how they vary, and how they interact.

## 4.1 On fractional vegetation cover

Low fractional vegetation cover is a primary limitation in detecting LSP in drylands [28]. There is high spatial and temporal variability in vegetation cover throughout arid regions. To highlight where vegetation cover is the limiting factor in LSP detection we calculated the average and standard deviation of total fractional vegetation cover in drylands in the western United States across 20 years (Figures 6 & 7). There is a general gradient of increasing fractional cover moving from south to north in deserts of the USA. The Sonoran and Mojave desert ecoregions have the lowest fractional cover, with median values of approximately 20%. In the northern regions there are large areas exceeding 60% fractional cover. Whether this translates to detectable phenology depends on the plant composition and resulting $VI_{veg}$ amplitudes. Even at 100% fractional cover there may be no LSP signal due to, for example, low $VI_{veg}$ amplitude in evergreen plants (Figure 2). These dynamics can result in confounding trends where there may be higher LSP detectability in areas with lower fractional vegetation cover.

Year to year variation in vegetation cover is highest in the Chihuahuan Desert ecoregion and portions of the Sonoran and Mojave deserts (Figure 7). Here there is high variability in the germination of annual plants as well as greenup of perennial grasses, both of which are driven by precipitation [40, 41]. Confounding this further is different timings of greenup among plant functional groups in response to precipitation, resulting in two distinct growing seasons [42–44]. The dynamics of this bi-model seasonality was not explored here, but can be accounted for with the correct methods [6, 45].

In the northern ecoregions there are large areas of high variability which can be attributed to agriculture [46]. Outside agricultural areas variation in annual cover in the northern ecoregions is likely driven by disturbance and subsequent changes in plant composition. Large swaths of the Snake River Plain and Central and Northern Basin and Range have high variability due to high severity fires and subsequent annual grass dominance [47, 48]. Here detectability of LSP may increase when annual grasses replace evergreen shrubs, since the latter have a lower seasonal amplitude [49].

Changing plant composition can lead to variability in cover and subsequent LSP detectability [50]. From the trends seen across desert ecoregions, changing composition must be considered on two time scales. The first is long-term changes due to disturbance and succession, as seen in northern ecoregions. The second is within year variation where the apparent fractional cover and greenness as seen by satellite sensors is a function of which plants have responded to abiotic drivers [51].

## 4.2 On seasonal amplitude expectations

The seasonal amplitude of plants, the difference in VI between dormancy and peak, drives LSP dynamics. A larger amplitude means that less fractional cover is needed to accurately detect pheno-

logical transitions. At the scale of an individual plant seasonal VI amplitude is driven by functional type and leaf area index (LAI).

Canopies of non-evergreen plants, such as grasses, forbs, and deciduous shrubs can have high seasonal amplitudes, since in the dormant season these canopies consist primarily of background soil, litter, and/or senesced vegetation. A higher canopy LAI can increase the seasonal amplitude further, up to an approximate LAI of 2, beyond which VI's tend to saturate [28]. This has implications for long term trends in LSP related to plant growth. Once a plant matures to the canopy LAI saturation point, only further horizontal growth can increase pixel level VI since vertical growth does not decrease overall soil cover [25, 26].

Evergreen plants will have relatively low seasonal amplitude, and thus require significant fractional cover to detect phenology. Assuming LAI remains relatively constant throughout the year then variation in the VI of evergreen plants depends solely on the structure and turnover of leaves, resulting in little to no seasonal amplitude. Indeed, studies of several evergreen shrubs found them to have seasonal amplitude of less than 0.1 NDVI units [25, 52]. Thus even when fractional cover approaches 100%, pixels with predominantly evergreen vegetation cannot have detectable phenology. Furthermore, pixels with high amounts of evergreen vegetation may occasionally have LSP detections solely by chance (ie. false positives) due to the inherent uncertainty in satellite imagery. Our simulation results show that the resulting phenological metrics in these scenarios, where the $VI_{pixel}$ amplitude rarely exceeds a QA threshold, can have errors of several weeks or more.

### 4.3 On VI uncertainty

VI uncertainty from shadows, view angle, and atmospheric interference can increase the false positive and false negative rates in LSP detections and increase errors in resulting transition dates [12]. False negatives can occur when a VI time series does not meet the QA threshold when it otherwise would with zero uncertainty. False positives can occur when a VI time series erroneously exceeds a QA threshold when it normally would not have with zero uncertainty. Our simulations show that increasing VI uncertainty increases false positives at low fractional cover, and increases false negatives at higher cover (Figure 3). Higher uncertainty also increases error in transition date estimates [53]. Our simulation results showed that increasing VI uncertainty increased the mean absolute error in all scenarios and metrics (Figure 4).

At intermediate levels of fractional vegetation cover VI uncertainty determines LSP detectability, whereas very high or very low fractional vegetation cover leads to a signal to noise ratio which makes VI uncertainty negligible. The upper threshold of fractional vegetation cover at which VI uncertainty becomes negligible for LSP detection depends on the seasonal VI amplitude of vegetation. Vegetation with high seasonal amplitude, such as deciduous plants with high LAI, have a lower threshold of fractional vegetation cover, above which VI uncertainty is negligible for LSP detection. LSP detection of vegetation with low seasonal amplitude, such as evergreen plants, is affected by VI uncertainty even at 100% fractional cover (Figure 2). Indeed, the combination of high VI uncertainty and evergreen dominated landscapes can lead to improbable winter peaks in greenness [54].

In our simulation analysis we characterized VI uncertainty as zero-centered gaussian noise with a

constant standard deviation of either 0.01 or 0.04. In reality the standard deviation of VI uncertainty can range from less than 0.01 to over 0.1 depending on the specific index used, its magnitude, and the sensor [55–57]. VI uncertainty can also vary between the dormant and growing season due to changing VI magnitude. Uncertainty decreases with increasing VI magnitude for NDVI and most other indices, while EVI uncertainty increases with higher EVI magnitude [55]. Differences in design, degradation, orbital drift, and spatial and spectral resolution lead to different VI uncertainties across sensors [55, 58]. Coarser spatial resolution decreases uncertainty [59], though this does not imply upscaling will produce more precise phenological estimates [8, 60, 61]. Data products which correct to surface reflectance have significantly lower uncertainty than top of atmosphere reflectance, though the uncertainty is still high enough to produce the patterns seen here [56].

## 4.4 On methodology

The algorithms used for LSP detection in drylands need further study, ideally to identify the underlying mechanism which makes one method more suitable than others. Using simulated, and idealized data we found a curvature method generally outperformed a threshold method except for EOS estimates of low $VI_{veg}$ amplitudes. This was likely the result of the gradual greendown in underlying double sigmoid used in the simulation analysis, where after adding VI uncertainty the steepest part of which was highly variable. With UAV imagery the threshold method produced lower MAE than the curvature method in most instances. This could be due to the low temporal density of only eight UAV flight dates throughout the year. With limited sample size the date of maximum change in the smoothed VI curve can be more variable than the date when a relative threshold is reached. Thus, any evaluation of algorithms for dryland LSP detection must also consider the temporal scale of the sensor in addition to the vegetation and VI attributes. The most suitable algorithm for UAV imagery in a particular ecosystem will not necessarily be the most suitable for satellite based imagery in the same ecosystem.

Other algorithmic improvements may also aid dryland LSP studies. For example methods which reduce VI uncertainty can be beneficial, since here we have shown this can decrease false positive and false negative detections and also increase the accuracy of the resulting transition date estimates. Propagation of VI uncertainty cannot improve LSP metrics directly, but can provide better context for transition date estimates through confidence intervals, which are rarely used in LSP trend studies [62]. VI uncertainty propagation is difficult to implement though [57], and would likely best be done as additions to Level 2 or higher data products.

## 4.5 On mixed pixels

The single vegetation type used in our simulation and UAV imagery analysis is likely rare in most drylands [63]. Mixed vegetation pixels complicate LSP in several ways beyond what we evaluated here. For example Chen et al. 2018 [50] found that, in a pixel with two vegetation types, the estimated green up date can vary solely due to changing species composition and not changing plant phenology. Dryland plant dynamics complicate LSP detection further since different functional types respond differently to precipitation pulses. For example grasses may green up sporadically, or even

not at all, due to the amount and timing of precipitation. Conversely surrounding shrubs, which access deeper water pools, can leaf out consistently every year [64–66]. Combined with low fractional cover this makes sparse vegetation drylands one of the hardest ecosystems for detecting LSP.

## 4.6 On low amplitude errors

Here we have highlighted a little studied aspect of LSP research. As $VI_{pixel}$ amplitude decreases, either from lower fractional vegetation cover or lower $VI_{veg}$ amplitude, potential error in transition date estimates increase. This is associated with the inherent parameter uncertainty in smoothing algorithms, leading to a statistical limitation in estimating transition dates. We illustrated this effect in Figure 8, where three VI curves have the same VI uncertainty (SD = 0.01) but different $VI_{pixel}$ amplitudes. As amplitude decreases, the potential range of onset dates increases. This happens with both a threshold- and curvature-based approach, though the curvature-based approach is less sensitive. As seen in both the simulation and UAV imagery analysis here this leads to higher error potential at lower $VI_{pixel}$ amplitudes. Confidence intervals, and errors of resulting transition date estimates, can be decreased with different temporal composite methods and/or with smaller temporal resolutions [67]. A best practice would also be to incorporate transition date confidence intervals into LSP studies for more appropriate statistical tests.

## 4.7 Moving Forward

Due to low seasonal amplitude the timing of seasonal transitions cannot be accurately estimated in many dryland areas with the current suite of satellite sensors and methodologies, though there is opportunity in some instances. Opportunities exist in areas with high spatial variation in vegetation type and cover, where small patches of vegetation meet or exceed the needed thresholds. In these areas finer resolution sensors (eg. Landsat & Sentinel-2) can potentially detect LSP where coarser resolution sensors (eg. MODIS, VIIRS, & AVHRR) cannot [49]. Another opportunity is infrequent "super blooms" which occur in several desert regions worldwide and have distinct VI signals [68]. High fractional cover of flowers require special consideration since they have lower VI values than green leaves, but still significantly higher than bare soil [69]. This is also an opportunity to upscale vegetation indices developed for flowers in agricultural areas [70, 71].

In areas where $VI_{veg}$ amplitude is extremely low the timing of peak greenness is likely the most suitable metric. Here we found estimates of peak greenness showed less bias than those for the start or end of season, especially when $VI_{veg}$ amplitude was low. Other studies have shown the timing and amplitude of peak greenness to be reliable in studying evergreen phenology [13, 72] and annual vegetation biomass [73]. Though caution must still be observed here since low $VI_{veg}$ amplitude can lead to improbable winter peaks [54].

With high-resolution sensors sparse vegetation can be advantageous in tracking phenology. Areas of open canopy, which are common in drylands, are the easiest environments for automatic identification of individual plants in high resolution imagery [74]. By combining high resolution imagery with frequent visits the phenology of individual plants can then be tracked. As opposed to landscape level variation in phenology of moderate resolution sensors, high resolution sensors could thus be

used to study phenology within and among species or across different microhabitats in drylands (e.g., [41]). The within canopy variation in VI, usually negligible at coarse resolutions, can affect LSP detectability. Though results from our UAV imagery analysis suggest that aggregating over all pixels within a plant canopy is likely adequate.

Similarly, UAV imagery can also be used to track phenology at the individual plant level. We found a potential shortcoming in using UAV imagery for LSP analysis, where the peak estimate had large errors relative to SOS and EOS estimates. This could be due to the true date of peak greenness being between our flight dates. Another possible cause is variation in timing of leaf maturity and senescence within the plant canopy, causing differences due to the oblique angle or categorical ocular estimates of in-situ observations compared to UAV imagery. Understory species within the mesquite canopy may drive an earlier peak when measured by UAV imagery. Thus when using UAV imagery to estimate phenology, one should maximize the number of sample dates, especially since peak greenness can only be estimated retrospectively. As high resolution imagery becomes more accessible and commonly used, the relationship between fine scale canopy attributes and how they relate to in-situ observations should be explored more [75, 76].

Other data products which are not proxies of greenness show promise in detecting dryland dynamics, since greenness is not always correlated with physiological activity [77]. Solar-Induced Chlorophyll Fluorescence (SIF) is theoretically not affected by high soil cover since soil is non-fluorescing [78, 79]. In practice SIF-derived LSP transition dates compared with in-situ observations have higher errors in areas with low vegetation cover, likely due to the low seasonal amplitude of the resulting annual time series [80]. Vegetation optical depth, derived from passive microwave sensors, is more sensitive to woody and herbaceous foliage than NDVI and can potentially help discriminate between them [21, 81]. Weather and climate data such as air and soil temperature and precipitation would likely be beneficial in constraining transition dates to biologically realistic ranges [54, 82, 83]. Integrating data from multiple sensor types, thereby retaining the relative advantages of each, shows promise in improving the detectability and accuracy of dryland LSP [21, 81, 84, 85].

The definition of LSP detectability, here whether a $VI_{pixel}$ amplitude exceeds 0.1 VI units, can potentially be improved. The 0.1 threshold is used in numerous studies, yet its origin and suitability is unclear. Here we showed that it indeed excludes instances where errors can be extremely high, yet does not fully minimize errors in all scenarios. A better methodology or framework for LSP detection could help in dryland LSP studies. For example, instead of whether a pixel amplitude exceeds an arbitrary threshold, detectability might be better defined as whether sensors could discern if plants actually exited dormancy. A false negative detection would then occur if plants within a pixel were deemed to have remained in dormancy, and no transition dates were estimated, when in fact there was plant growth and/or productivity. Theoretically this would make detectability invariant to fractional vegetation cover. Re-framing the detectability of LSP like this, or in other substantial ways, can lead to more innovative research for studying dryland LSP.

# 5 Conclusion

Drylands constitute approximately 41% of the Earth's surface [86] and their high variability in annual productivity plays an important role in global terrestrial net primary productivity [87]. For these reasons, it is important to understand underlying factors limiting LSP studies in drylands. We found that the interaction of fractional vegetation cover and seasonal VI amplitude of plant canopies are the primary drivers of dryland LSP detectability and accuracy. At intermediate levels of fractional vegetation cover VI uncertainty associated with shadows, atmospheric interference, and view angle affects detectability. Retrospective studies will always be limited in their ability to measure LSP in drylands due to coarse resolution sensors. Full uncertainty propagation, from sensor measurement to statistical models, can help contextualize results in any LSP study, but is especially pertinent for drylands. High resolution sensors are the most promising path forward for measuring LSP in drylands since sparse vegetation is advantageous for identification of individual plants. Drylands thus have the potential to become an exemplary environment for future LSP research.

## Acknowledgments

This research was a contribution from the Long-Term Agroecosystem Research (LTAR) network. LTAR is supported by the United States Department of Agriculture. DMB and RAB were supported by CRIS #3050-11210-009-00D. We acknowledge the Jornada Basin Long-Term Ecological Research (LTER) site for sustaining the long-term research location (DEB 20-25166). The authors acknowledge the USDA Agricultural Research Service (ARS) Big Data Initiative and SCINet high performance computing resources (https://scinet.usda.gov) and funding from the Scientific Computing Initiative (SCINet) Postdoctoral Fellow program to support SDT. Any use of trade, firm, or product names is for descriptive purposes only and does not imply endorsement by the U.S. Government. USDA is an equal opportunity provider and employer.

## Author Contributions

S.D. Taylor performed the analysis and wrote the manuscript with guidance from D.M. Browning. R. Baca collected and processed the UAV imagery and phenology data. D.M. Browning and F. Gao provided important comments and revised the manuscript.

# 6 Bibliography

## References

[1] X. Zhang, L. Liu, Y. Liu, S. Jayavelu, J. Wang, M. Moon, G. M. Henebry, M. A. Friedl, and C. B. Schaaf, "Generation and evaluation of the viirs land surface phenology product," *Remote Sensing of Environment*, vol. 216, pp. 212–229, Oct. 2018, ISSN: 00344257. DOI: 10.1016/j.rse.2018.06.047.

[2] M. Friedl, G. M. Henebry, B. Reed, A. Huete, M. White, J. Morisette, R. Nemani, X. Zhang, and R. Myneni, "Land surface phenology: A community white paper requested by nasa," Tech. Rep., 2006. [Online]. Available: https://cce.nasa.gov/mtg2008_ab_presentations/Phenology_Friedl_whitepaper.pdf.

[3] P. Jönsson and L. Eklundh, "Timesat—a program for analyzing time-series of satellite sensor data," *Computers & Geosciences*, vol. 30, no. 8, pp. 833–845, Oct. 2004, ISSN: 00983004. DOI: 10.1016/j.cageo.2004.05.006.

[4] T. Sakamoto, B. D. Wardlow, A. A. Gitelson, S. B. Verma, A. E. Suyker, and T. J. Arkebauer, "A two-step filtering approach for detecting maize and soybean phenology with time-series modis data," *Remote Sensing of Environment*, vol. 114, no. 10, pp. 2146–2159, Oct. 2010, ISSN: 00344257. DOI: 10.1016/j.rse.2010.04.019.

[5] F. Gao, M. C. Anderson, X. Zhang, Z. Yang, J. G. Alfieri, W. P. Kustas, R. Mueller, D. M. Johnson, and J. H. Prueger, "Toward mapping crop progress at field scales through fusion of landsat and modis imagery," *Remote Sensing of Environment*, vol. 188, pp. 9–25, Jan. 2017, ISSN: 00344257. DOI: 10.1016/j.rse.2016.11.004.

[6] J. Gray, D. Sulla-Menashe, and M. A. Friedl, "User guide to collection 6 modis land cover dynamics (mcd12q2) product," *User Guide*, vol. 6, pp. 1–8, 2019.

[7] D. K. Bolton, J. M. Gray, E. K. Melaas, M. Moon, L. Eklundh, and M. A. Friedl, "Continental-scale land surface phenology from harmonized landsat 8 and sentinel-2 imagery," *Remote Sensing of Environment*, vol. 240, p. 111 685, Apr. 2020, ISSN: 00344257. DOI: 10.1016/j.rse.2020.111685.

[8] L. Zeng, B. D. Wardlow, D. Xiang, S. Hu, and D. Li, "A review of vegetation phenological metrics extraction using time-series, multispectral satellite data," *Remote Sensing of Environment*, vol. 237, no. November 2019, p. 111 511, Feb. 2020, ISSN: 00344257. DOI: 10.1016/j.rse.2019.111511.

[9] S. Piao, X. Wang, T. Park, C. Chen, X. Lian, Y. He, J. W. Bjerke, A. Chen, P. Ciais, H. Tømmervik, R. R. Nemani, and R. B. Myneni, "Characteristics, drivers and feedbacks of global greening," *Nature Reviews Earth & Environment*, vol. 1, no. 1, pp. 14–27, Jan. 2020, ISSN: 2662-138X. DOI: 10.1038/s43017-019-0001-x.

[10] A. D. Richardson, K. Hufkens, T. Milliman, and S. Frolking, "Intercomparison of phenological transition dates derived from the phenocam dataset v1.0 and modis satellite remote sensing," *Scientific Reports*, vol. 8, no. 1, p. 5679, Dec. 2018, ISSN: 20452322. DOI: 10.1038/s41598-018-23804-6.

[11] M. A. White, K. M. de Beurs, K. Didan, D. W. Inouye, A. D. Richardson, O. P. Jensen, J. O'Keefe, G. Zhang, R. R. Nemani, W. J. van Leeuwen, J. F. Brown, A. de Wit, M. Schaepman, X. Lin, M. Dettinger, A. S. Bailey, J. Kimball, M. D. Schwartz, D. D. Baldocchi, J. T. Lee, and W. K. Lauenroth, "Intercomparison, interpretation, and assessment of spring phenology in north america estimated from remote sensing for 1982-2006," *Global Change Biology*, vol. 15, no. 10, pp. 2335–2359, Oct. 2009, ISSN: 13541013. DOI: 10.1111/j.1365-2486.2009.01910.x.

[12] X. Ma, A. Huete, Q. Yu, N. R. Coupe, K. Davies, M. Broich, P. Ratana, J. Beringer, L. B. Hutley, J. Cleverly, N. Boulain, and D. Eamus, "Spatial patterns and temporal dynamics in savanna vegetation phenology across the north australian tropical transect," *Remote Sensing of Environment*, vol. 139, pp. 97–115, Dec. 2013, ISSN: 00344257. DOI: 10.1016/j.rse.2013.07.030.

[13] J. Walker, K. de Beurs, and R. H. Wynne, "Phenological response of an arizona dryland forest to short-term climatic extremes," *Remote Sensing*, vol. 7, no. 8, pp. 10 832–10 855, Aug. 2015, ISSN: 20724292. DOI: 10.3390/rs70810832.

[14] S. J. Jeong, C. H. Ho, H. J. Gim, and M. E. Brown, "Phenology shifts at start vs. end of growing season in temperate vegetation over the northern hemisphere for the period 1982-2008," *Global Change Biology*, vol. 17, no. 7, pp. 2385–2399, Jul. 2011, ISSN: 13541013. DOI: 10.1111/j.1365-2486.2011.02397.x.

[15] W. Zhu, H. Tian, X. Xu, Y. Pan, G. Chen, and W. Lin, "Extension of the growing season due to delayed autumn over mid and high latitudes in north america during 1982-2006," *Global Ecology and Biogeography*, vol. 21, no. 2, pp. 260–271, Feb. 2012, ISSN: 1466822X. DOI: 10.1111/j.1466-8238.2011.00675.x.

[16] M. Shen, G. Zhang, N. Cong, S. Wang, W. Kong, and S. Piao, "Increasing altitudinal gradient of spring vegetation phenology during the last decade on the qinghai-tibetan plateau," *Agricultural and Forest Meteorology*, vol. 189-190, pp. 71–80, Jun. 2014, ISSN: 01681923. DOI: 10.1016/j.agrformet.2014.01.003.

[17] Q. Xin, M. Broich, P. Zhu, and P. Gong, "Modeling grassland spring onset across the western united states using climate variables and modis-derived phenology metrics," *Remote Sensing of Environment*, vol. 161, pp. 63–77, May 2015, ISSN: 00344257. DOI: 10.1016/j.rse.2015.02.003.

[18] I. Garonna, R. de Jong, and M. E. Schaepman, "Variability and evolution of global land surface phenology over the past three decades (1982-2012)," *Global Change Biology*, vol. 22, no. 4, pp. 1456–1468, Apr. 2016, ISSN: 13652486. DOI: 10.1111/gcb.13168.

[19] J. Hou, L. Du, K. Liu, Y. Hu, and Y. Zhu, "Characteristics of vegetation activity and its responses to climate change in desert/grassland biome transition zones in the last 30 years based on gimms3g," *Theoretical and Applied Climatology*, vol. 136, no. 3-4, pp. 915–928, May 2019, ISSN: 14344483. DOI: 10.1007/s00704-018-2527-0.

[20] R. Fensholt, T. Langanke, K. Rasmussen, A. Reenberg, S. D. Prince, C. Tucker, R. J. Scholes, Q. B. Le, A. Bondeau, R. Eastman, H. Epstein, A. E. Gaughan, U. Hellden, C. Mbow, L. Olsson, J. Paruelo, C. Schweitzer, J. Seaquist, and K. Wessels, "Greenness in semi-arid areas across the globe 1981-2007 - an earth observing satellite based analysis of trends and drivers," *Remote Sensing of Environment*, vol. 121, pp. 144–158, Jun. 2012, ISSN: 00344257. DOI: 10.1016/j.rse.2012.01.017.

[21] N. Andela, Y. Y. Liu, A. I. M. Van Dijk, R. A. De Jeu, and T. R. McVicar, "Global changes in dryland vegetation dynamics (1988-2008) assessed by satellite remote sensing: Comparing a new passive microwave vegetation density record with reflective greenness data," *Biogeosciences*, vol. 10, no. 10, pp. 6657–6676, Oct. 2013, ISSN: 17264170. DOI: 10.5194/bg-10-6657-2013.

[22] A. Huete, C. Justice, and H. Liu, "Development of vegetation and soil indices for modis-eos," *Remote Sensing of Environment*, vol. 49, no. 3, pp. 224–234, Sep. 1994, ISSN: 00344257. DOI: 10.1016/0034-4257(94)90018-3.

[23] Z. Jiang, A. R. Huete, J. Chen, Y. Chen, J. Li, G. Yan, and X. Zhang, "Analysis of ndvi and scaled difference vegetation index retrievals of vegetation fraction," *Remote Sensing of Environment*, vol. 101, no. 3, pp. 366–378, Apr. 2006, ISSN: 00344257. DOI: 10.1016/j.rse.2006.01.003.

[24] A. J. Elmore, S. M. Guinn, B. J. Minsley, and A. D. Richardson, "Landscape controls on the timing of spring, autumn, and growing season length in mid-atlantic forests," *Global Change Biology*, vol. 18, no. 2, pp. 656–674, Feb. 2012, ISSN: 13541013. DOI: 10.1111/j.1365-2486.2011.02521.x.

[25] J. A. Gamon, C. B. Field, M. L. Goulden, K. L. Griffin, A. E. Hartley, G. Joel, J. Penuelas, and R. Valentini, "Relationships between ndvi, canopy structure, and photosynthesis in three californian vegetation types," *Ecological Applications*, vol. 5, no. 1, pp. 28–41, Feb. 1995, ISSN: 10510761. DOI: 10.2307/1942049.

[26] T. N. Carlson and D. A. Ripley, "On the relation between ndvi, fractional vegetation cover, and leaf area index," *Remote Sensing of Environment*, vol. 62, no. 3, pp. 241–252, Dec. 1997, ISSN: 00344257. DOI: 10.1016/S0034-4257(97)00104-1.

[27] M. Baghzouz, D. A. Devitt, L. F. Fenstermaker, and M. H. Young, "Monitoring vegetation phenological cycles in two different semi-arid environmental settings using a ground-based ndvi system: A potential approach to improve satellite data interpretation," *Remote Sensing*, vol. 2, no. 4, pp. 990–1013, Apr. 2010, ISSN: 20724292. DOI: 10.3390/rs2040990.

[28] W. K. Smith, M. P. Dannenberg, D. Yan, S. Herrmann, M. L. Barnes, G. A. Barron-Gafford, J. A. Biederman, S. Ferrenberg, A. M. Fox, A. Hudson, J. F. Knowles, N. MacBean, D. J. Moore, P. L. Nagler, S. C. Reed, W. A. Rutherford, R. L. Scott, X. Wang, and J. Yang, "Remote sensing of dryland ecosystem structure and function: Progress, challenges, and opportunities," *Remote Sensing of Environment*, vol. 233, no. October, p. 111 401, Nov. 2019, ISSN: 00344257. DOI: 10.1016/j.rse.2019.111401.

[29] A. R. Huete and R. D. Jackson, "Suitability of spectral indices for evaluating vegetation characteristics on arid rangelands," *Remote Sensing of Environment*, vol. 23, no. 2, 213–IN8, Nov. 1987, ISSN: 00344257. DOI: 10.1016/0034-4257(87)90038-1.

[30] M. P. Dannenberg and E. K. Wise, "Shifting pacific storm tracks as stressors to ecosystems of western north america," *Global Change Biology*, vol. 23, no. 11, pp. 4896–4906, Nov. 2017, ISSN: 13652486. DOI: 10.1111/gcb.13748.

[31] D. M. Browning, A. Rango, J. W. Karl, C. M. Laney, E. R. Vivoni, and C. E. Tweedie, "Emerging technological and cultural shifts advancing drylands research and management," *Frontiers in Ecology and the Environment*, vol. 13, no. 1, pp. 52–60, Feb. 2015, ISSN: 15409309. DOI: 10.1890/140161.

[32] S. Cao, B. Danielson, S. Clare, S. Koenig, C. Campos-Vargas, and A. Sanchez-Azofeifa, "Radiometric calibration assessments for uas-borne multispectral cameras: Laboratory and field protocols," *ISPRS Journal of Photogrammetry and Remote Sensing*, vol. 149, no. January, pp. 132–145, Mar. 2019, ISSN: 09242716. DOI: 10.1016/j.isprsjprs.2019.01.016.

[33] A. H. Strahler, C. E. Woodcock, and J. A. Smith, "On the nature of models in remote sensing," *Remote Sensing of Environment*, vol. 20, no. 2, pp. 121–139, Oct. 1986, ISSN: 00344257. DOI: 10.1016/0034-4257(86)90018-0.

[34] F. Gao and X. Zhang, "Mapping crop phenology in near real-time using satellite remote sensing: Challenges and opportunities," *Journal of Remote Sensing*, vol. 2021, pp. 1–14, Mar. 2021, ISSN: 2694-1589. DOI: 10.34133/2021/8379391.

[35] X. Zhang, M. A. Friedl, C. B. Schaaf, A. H. Strahler, J. C. Hodges, F. Gao, B. C. Reed, and A. Huete, "Monitoring vegetation phenology using modis," *Remote Sensing of Environment*, vol. 84, no. 3, pp. 471–475, Mar. 2003, ISSN: 00344257. DOI: 10.1016/S0034-4257(02)00135-9.

[36] F. Gao, M. Anderson, C. Daughtry, A. Karnieli, D. Hively, and W. Kustas, "A within-season approach for detecting early growth stages in corn and soybean using high temporal and spatial resolution imagery," *Remote Sensing of Environment*, vol. 242, p. 111 752, Jun. 2020, ISSN: 00344257. DOI: 10.1016/j.rse.2020.111752.

[37] F. Gao, M. C. Anderson, and W. D. Hively, "Detecting cover crop end-of-season using venµs and sentinel-2 satellite imagery," *Remote Sensing*, vol. 12, no. 21, p. 3524, Oct. 2020, ISSN: 2072-4292. DOI: 10.3390/rs12213524.

[38] X. Zhang, M. D. Goldberg, and Y. Yu, "Prototype for monitoring and forecasting fall foliage coloration in real time from satellite data," *Agricultural and Forest Meteorology*, vol. 158-159, pp. 21–29, Jun. 2012, ISSN: 01681923. DOI: 10.1016/j.agrformet.2012.01.013.

[39] L. Liu, X. Zhang, Y. Yu, F. Gao, and Z. Yang, "Real-time monitoring of crop phenology in the midwestern united states using viirs observations," *Remote Sensing*, vol. 10, no. 10, p. 1540, Sep. 2018, ISSN: 2072-4292. DOI: 10.3390/rs10101540.

[40] J. C. Beatley, "Phenological events and their environmental triggers in mojave desert ecosystems," *Ecology*, vol. 55, no. 4, pp. 856–863, Jul. 1974, ISSN: 1095-922X. DOI: 10.2307/1934421.

[41] D. M. Browning, J. W. Karl, D. Morin, A. D. Richardson, and C. E. Tweedie, "Phenocams bridge the gap between field and satellite observations in an arid grassland ecosystem," *Remote Sensing*, vol. 9, no. 10, p. 1071, Oct. 2017, ISSN: 20724292. DOI: 10.3390/rs9101071.

[42] S. K. M. Ernest, J. H. Brown, and R. R. Parmenter, "Rodents, plants, and precipitation: Spatial and temporal dynamics of consumers and resources," *Oikos*, vol. 88, no. 3, pp. 470–482, Mar. 2000, ISSN: 00301299. DOI: 10.1034/j.1600-0706.2000.880302.x.

[43] J. L. Weiss, D. S. Gutzler, J. E. Coonrod, and C. N. Dahm, "Long-term vegetation monitoring with ndvi in a diverse semi-arid setting, central new mexico, usa," *Journal of Arid Environments*, vol. 58, no. 2, pp. 249–272, Jul. 2004, ISSN: 01401963. DOI: 10.1016/j.jaridenv.2003.07.001.

[44] D. M. Browning, T. M. Crimmins, D. K. James, S. Spiegal, M. R. Levi, J. P. Anderson, and D. P. Peters, "Synchronous species responses reveal phenological guilds: Implications for management," *Ecosphere*, vol. 9, no. 9, e02395, Sep. 2018, ISSN: 21508925. DOI: 10.1002/ecs2.2395.

[45] R. Buitenwerf, L. Rose, and S. I. Higgins, "Three decades of multi-dimensional change in global leaf phenology," *Nature Climate Change*, vol. 5, no. 4, pp. 364–368, Apr. 2015, ISSN: 17586798. DOI: 10.1038/nclimate2533.

[46] B. A. Bradley and J. F. Mustard, "Comparison of phenology trends by land cover class: A case study in the great basin, usa," *Global Change Biology*, vol. 14, no. 2, pp. 334–346, Feb. 2008, ISSN: 13541013. DOI: 10.1111/j.1365-2486.2007.01479.x.

[47] B. A. Bradley, C. A. Curtis, E. J. Fusco, J. T. Abatzoglou, J. K. Balch, S. Dadashi, and M. N. Tuanmu, "Cheatgrass (bromus tectorum) distribution in the intermountain western united states and its relationship to fire frequency, seasonality, and ignitions," *Biological Invasions*, vol. 20, no. 6, pp. 1493–1506, Jun. 2018, ISSN: 15731464. DOI: 10.1007/s10530-017-1641-8.

[48] N. J. Pastick, D. Dahal, B. K. Wylie, S. Parajuli, S. P. Boyte, and Z. Wu, "Characterizing land surface phenology and exotic annual grasses in dryland ecosystems using landsat and sentinel-2 data in harmony," *Remote Sensing*, vol. 12, no. 4, p. 725, Feb. 2020, ISSN: 2072-4292. DOI: 10.3390/rs12040725.

[49] D. Peng, Y. Wang, G. Xian, A. R. Huete, W. Huang, M. Shen, F. Wang, L. Yu, L. Liu, Q. Xie, L. Liu, and X. Zhang, "Investigation of land surface phenology detections in shrublands using multiple scale satellite data," *Remote Sensing of Environment*, vol. 252, no. April 2020, p. 112 133, Jan. 2021, ISSN: 00344257. DOI: 10.1016/j.rse.2020.112133.

[50] X. Chen, D. Wang, J. Chen, C. Wang, and M. Shen, "The mixed pixel effect in land surface phenology: A simulation study," *Remote Sensing of Environment*, vol. 211, no. March, pp. 338–344, Jun. 2018, ISSN: 00344257. DOI: 10.1016/j.rse.2018.04.030.

[51] D. Helman, "Land surface phenology: What do we really 'see' from space?" *Science of the Total Environment*, vol. 618, pp. 665–673, Mar. 2018, ISSN: 18791026. DOI: 10.1016/j.scitotenv.2017.07.237.

[52] C. D. Stylinski, J. A. Gamon, and W. C. Oechel, "Seasonal patterns of reflectance indices, carotenoid pigments and photosynthesis of evergreen chaparral species," *Oecologia*, vol. 131, no. 3, pp. 366–374, May 2002, ISSN: 00298549. DOI: 10.1007/s00442-002-0905-9.

[53] X. Ma, A. Huete, and N. N. Tran, "Interaction of seasonal sun-angle and savanna phenology observed and modelled using modis," *Remote Sensing*, vol. 11, no. 12, p. 1398, Jun. 2019, ISSN: 20724292. DOI: 10.3390/rs11121398.

[54] J. R. Norris and J. J. Walker, "Solar and sensor geometry, not vegetation response, drive satellite ndvi phenology in widespread ecosystems of the western united states," *Remote Sensing of Environment*, vol. 249, p. 112 013, Nov. 2020, ISSN: 00344257. DOI: 10.1016/j.rse.2020.112013.

[55] T. Miura, "Evaluation of sensor calibration uncertainties on vegetation indices for modis," *IEEE Transactions on Geoscience and Remote Sensing*, vol. 38, no. 3, pp. 1399–1409, May 2000, ISSN: 01962892. DOI: 10.1109/36.843034.

[56] J. R. Nagol, E. F. Vermote, and S. D. Prince, "Effects of atmospheric variation on avhrr ndvi data," *Remote Sensing of Environment*, vol. 113, no. 2, pp. 392–397, Feb. 2009, ISSN: 00344257. DOI: 10.1016/j.rse.2008.10.007.

[57] E. Borgogno-Mondino, A. Lessio, and M. A. Gomarasca, "A fast operative method for ndvi uncertainty estimation and its role in vegetation analysis," *European Journal of Remote Sensing*, vol. 49, no. 1, pp. 137–156, Jan. 2016, ISSN: 22797254. DOI: 10.5721/EuJRS20164908.

[58] X. Fan and Y. Liu, "A comparison of ndvi intercalibration methods," *International Journal of Remote Sensing*, vol. 38, no. 19, pp. 5273–5290, Oct. 2017, ISSN: 13665901. DOI: 10.1080/01431161.2017.1338784.

[59] W. Chen, P. Zorn, Z. Chen, R. Latifovic, Y. Zhang, J. Li, J. Quirouette, I. Olthof, R. Fraser, D. Mclennan, J. Poitevin, H. M. Stewart, and R. Sharma, "Propagation of errors associated with scaling foliage biomass from field measurements to remote sensing data over a northern canadian national park," *Remote Sensing of Environment*, vol. 130, pp. 205–218, Mar. 2013, ISSN: 00344257. DOI: 10.1016/j.rse.2012.11.012.

[60] X. Zhang, J. Wang, F. Gao, Y. Liu, C. Schaaf, M. Friedl, Y. Yu, S. Jayavelu, J. Gray, L. Liu, D. Yan, and G. M. Henebry, "Exploration of scaling effects on coarse resolution land surface phenology," *Remote Sensing of Environment*, vol. 190, pp. 318–330, Mar. 2017, ISSN: 00344257. DOI: 10.1016/j.rse.2017.01.001.

[61] D. Peng, X. Zhang, B. Zhang, L. Liu, X. Liu, A. R. Huete, W. Huang, S. Wang, S. Luo, X. Zhang, and H. Zhang, "Scaling effects on spring phenology detections from modis data at multiple spatial resolutions over the contiguous united states," *ISPRS Journal of Photogrammetry and Remote Sensing*, vol. 132, pp. 185–198, Oct. 2017, ISSN: 09242716. DOI: 10.1016/j.isprsjprs.2017.09.002.

[62] J. Cortés, M. D. Mahecha, M. Reichstein, R. B. Myneni, C. Chen, and A. Brenning, "Where are global vegetation greening and browning trends significant?" *Geophysical Research Letters*, vol. 48, no. 6, Mar. 2021, ISSN: 0094-8276. DOI: 10.1029/2020gl091496.

[63] M. O. Jones, B. W. Allred, D. E. Naugle, J. D. Maestas, P. Donnelly, L. J. Metz, J. Karl, R. Smith, B. Bestelmeyer, C. Boyd, J. D. Kerby, and J. D. McIver, "Innovation in rangeland monitoring: Annual, 30 m, plant functional type percent cover maps for u.s. rangelands, 1984–2017," *Ecosphere*, vol. 9, no. 9, e02430, Sep. 2018, ISSN: 21508925. DOI: 10.1002/ecs2.2430.

[64] K. Ogle and J. F. Reynolds, "Plant responses to precipitation in desert ecosystems: Integrating functional types, pulses, thresholds, and delays," *Oecologia*, vol. 141, no. 2, pp. 282–294, Oct. 2004, ISSN: 00298549. DOI: 10.1007/s00442-004-1507-5.

[65] W. K. Lauenroth, D. R. Schlaepfer, and J. B. Bradford, "Ecohydrology of dry regions: Storage versus pulse soil water dynamics," *Ecosystems*, vol. 17, no. 8, pp. 1469–1479, Dec. 2014, ISSN: 14350629. DOI: 10.1007/s10021-014-9808-y.

[66] M. Moreno-De Las Heras, R. Díaz-Sierra, L. Turnbull, and J. Wainwright, "Assessing vegetation structure and anpp dynamics in a grassland-shrubland chihuahuan ecotone using ndvi-rainfall relationships," *Biogeosciences*, vol. 12, no. 10, pp. 2907–2925, May 2015, ISSN: 17264189. DOI: 10.5194/bg-12-2907-2015.

[67] X. Zhang, M. A. Friedl, and C. B. Schaaf, "Sensitivity of vegetation phenology detection to the temporal resolution of satellite data," *International Journal of Remote Sensing*, vol. 30, no. 8, pp. 2061–2074, Apr. 2009, ISSN: 0143-1161. DOI: 10.1080/01431160802549237.

[68] R. Chávez, A. Moreira-Muñoz, M. Galleguillos, M. Olea, J. Aguayo, A. Latín, I. Aguilera-Betti, A. Muñoz, and H. Manríquez, "GIMMS NDVI time series reveal the extent, duration, and intensity of "blooming desert" events in the hyper-arid Atacama Desert, Northern Chile," *International Journal of Applied Earth Observation and Geoinformation*, vol. 76, no. December 2018, pp. 193–203, Apr. 2019, ISSN: 03032434. DOI: 10.1016/j.jag.2018.11.013. [Online]. Available: https://linkinghub.elsevier.com/retrieve/pii/S0303243418306202.

[69] M. Shen, J. Chen, X. Zhu, and Y. Tang, "Yellow flowers can decrease ndvi and evi values: Evidence from a field experiment in an alpine meadow," *Canadian Journal of Remote Sensing*, vol. 35, no. 2, pp. 99–106, Jan. 2009, ISSN: 17127971. DOI: 10.5589/m09-003.

[70] D. J. Dixon, J. N. Callow, J. M. Duncan, S. A. Setterfield, and N. Pauli, "Satellite prediction of forest flowering phenology," *Remote Sensing of Environment*, vol. 255, p. 112 197, Mar. 2021, ISSN: 00344257. DOI: 10.1016/j.rse.2020.112197.

[71] B. Chen, Y. Jin, and P. Brown, "An enhanced bloom index for quantifying floral phenology using multi-scale remote sensing observations," *ISPRS Journal of Photogrammetry and Remote Sensing*, vol. 156, no. April, pp. 108–120, Oct. 2019, ISSN: 09242716. DOI: 10.1016/j.isprsjprs.2019.08.006.

[72] J. J. Walker, K. M. de Beurs, and R. H. Wynne, "Dryland vegetation phenology across an elevation gradient in arizona, usa, investigated with fused modis and landsat data," *Remote Sensing of Environment*, vol. 144, pp. 85–97, Mar. 2014, ISSN: 00344257. DOI: 10.1016/j.rse.2014.01.007.

[73] G. Casady, W. van Leeuwen, and B. Reed, "Estimating Winter Annual Biomass in the Sonoran and Mojave Deserts with Satellite- and Ground-Based Observations," *Remote Sensing*, vol. 5, no. 2, pp. 909–926, Feb. 2013, ISSN: 2072-4292. DOI: 10.3390/rs5020909. [Online]. Available: http://www.mdpi.com/2072-4292/5/2/909.

[74] B. G. Weinstein, S. Marconi, S. A. Bohlman, A. Zare, and E. P. White, "Cross-site learning in deep learning rgb tree crown detection," *Ecological Informatics*, vol. 56, p. 101 061, Mar. 2020, ISSN: 15749541. DOI: 10.1016/j.ecoinf.2020.101061.

[75] S. Klosterman, E. Melaas, J. Wang, A. Martinez, S. Frederick, J. O'Keefe, D. A. Orwig, Z. Wang, Q. Sun, C. Schaaf, M. Friedl, and A. D. Richardson, "Fine-scale perspectives on landscape phenology from unmanned aerial vehicle (uav) photography," *Agricultural and Forest Meteorology*, vol. 248, pp. 397–407, Jan. 2018, ISSN: 01681923. DOI: 10.1016/j.agrformet.2017.10.015.

[76] Y. Cheng, A. Vrieling, F. Fava, M. Meroni, M. Marshall, and S. Gachoki, "Phenology of short vegetation cycles in a kenyan rangeland from planetscope and sentinel-2," *Remote Sensing of Environment*, vol. 248, p. 112 004, Oct. 2020, ISSN: 00344257. DOI: 10.1016/j.rse.2020.112004.

[77] S. J. Jeong, D. Schimel, C. Frankenberg, D. T. Drewry, J. B. Fisher, M. Verma, J. A. Berry, J. E. Lee, and J. Joiner, "Application of satellite solar-induced chlorophyll fluorescence to understanding large-scale variations in vegetation phenology and function over northern high latitude forests," *Remote Sensing of Environment*, vol. 190, pp. 178–187, Mar. 2017, ISSN: 00344257. DOI: 10.1016/j.rse.2016.11.021.

[78] C. Frankenberg, C. O'Dell, J. Berry, L. Guanter, J. Joiner, P. Köhler, R. Pollock, and T. E. Taylor, "Prospects for chlorophyll fluorescence remote sensing from the orbiting carbon observatory-2," *Remote Sensing of Environment*, vol. 147, pp. 1–12, May 2014, ISSN: 00344257. DOI: 10.1016/j.rse.2014.02.007.

[79] W. K. Smith, J. A. Biederman, R. L. Scott, D. J. Moore, M. He, J. S. Kimball, D. Yan, A. Hudson, M. L. Barnes, N. MacBean, A. M. Fox, and M. E. Litvak, "Chlorophyll fluorescence better captures seasonal and interannual gross primary productivity dynamics across dryland ecosystems of southwestern north america," *Geophysical Research Letters*, vol. 45, no. 2, pp. 748–757, Jan. 2018, ISSN: 19448007. DOI: 10.1002/2017GL075922.

[80] C. Wang, J. Beringer, L. B. Hutley, J. Cleverly, J. Li, Q. Liu, and Y. Sun, "Phenology dynamics of dryland ecosystems along the north australian tropical transect revealed by satellite solar-induced chlorophyll fluorescence," *Geophysical Research Letters*, vol. 46, no. 10, pp. 5294–5302, May 2019, ISSN: 19448007. DOI: 10.1029/2019GL082716.

[81] F. Tian, M. Brandt, Y. Y. Liu, A. Verger, T. Tagesson, A. A. Diouf, K. Rasmussen, C. Mbow, Y. Wang, and R. Fensholt, "Remote sensing of vegetation dynamics in drylands: Evaluating vegetation optical depth (vod) using avhrr ndvi and in situ green biomass data over west african sahel," *Remote Sensing of Environment*, vol. 177, pp. 265–276, May 2016, ISSN: 00344257. DOI: 10.1016/j.rse.2016.02.056.

[82] A. Hudson Dunn and K. M. de Beurs, "Land surface phenology of north american mountain environments using moderate resolution imaging spectroradiometer data," *Remote Sensing of Environment*, vol. 115, no. 5, pp. 1220–1233, May 2011, ISSN: 00344257. DOI: 10.1016/j.rse.2011.01.005.

[83] L. Liu, L. Liu, L. Liang, A. Donnelly, I. Park, and M. D. Schwartz, "Effects of elevation on spring phenological sensitivity to temperature in tibetan plateau grasslands," *Chinese Science Bulletin*, vol. 59, no. 34, pp. 4856–4863, Dec. 2014, ISSN: 1001-6538. DOI: 10.1007/s11434-014-0476-2.

[84] J. Wang, X. Xiao, R. Bajgain, P. Starks, J. Steiner, R. B. Doughty, and Q. Chang, "Estimating leaf area index and aboveground biomass of grazing pastures using sentinel-1, sentinel-2 and landsat images," *ISPRS Journal of Photogrammetry and Remote Sensing*, vol. 154, pp. 189–201, Aug. 2019, ISSN: 09242716. DOI: 10.1016/j.isprsjprs.2019.06.007.

[85] M. Dannenberg, X. Wang, D. Yan, and W. Smith, "Phenological characteristics of global ecosystems based on optical, fluorescence, and microwave remote sensing," *Remote Sensing*, vol. 12, no. 4, p. 671, Feb. 2020, ISSN: 2072-4292. DOI: 10.3390/rs12040671.

[86] D. L. Hoover, B. Bestelmeyer, N. B. Grimm, T. E. Huxman, S. C. Reed, O. Sala, T. R. Seastedt, H. Wilmer, and S. Ferrenberg, "Traversing the wasteland: A framework for assessing ecological threats to drylands," *BioScience*, vol. 70, no. 1, pp. 35–47, Jan. 2020, ISSN: 0006-3568. DOI: 10.1093/biosci/biz126.

[87] A. Ahlstrom, M. R. Raupach, G. Schurgers, B. Smith, A. Arneth, M. Jung, M. Reichstein, J. G. Canadell, P. Friedlingstein, A. K. Jain, E. Kato, B. Poulter, S. Sitch, B. D. Stocker, N. Viovy, Y. P. Wang, A. Wiltshire, S. Zaehle, and N. Zeng, "The dominant role of semi-arid ecosystems in the trend and variability of the land co2 sink," *Science*, vol. 348, no. 6237, pp. 895–899, May 2015, ISSN: 0036-8075. DOI: 10.1126/science.aaa1668.

[88] B. W. Allred, B. T. Bestelmeyer, C. S. Boyd, C. Brown, K. W. Davies, M. C. Duniway, L. M. Ellsworth, T. A. Erickson, S. D. Fuhlendorf, T. V. Griffiths, V. Jansen, M. O. Jones, J. Karl, A. Knight, J. D. Maestas, J. J. Maynard, S. E. McCord, D. E. Naugle, H. D. Starns, D. Twidwell, and D. R. Uden, "Improving landsat predictions of rangeland fractional cover with multitask learning and uncertainty," *Methods in Ecology and Evolution*, R. Freckleton, Ed., pp. 2041–210X.13564, Feb. 2021, ISSN: 2041210X. DOI: 10.1111/2041-210X.13564.

# Figures

# Supplementary Materials

- Figure S1: UAV imagery from July 5, 2019 at the Jornada Experimental Range NORT site used in this study.
- Figure S2: NDVI variation within mesquite shrub canopies.
- Figure S3: Example NDVI curves from UAV imagery

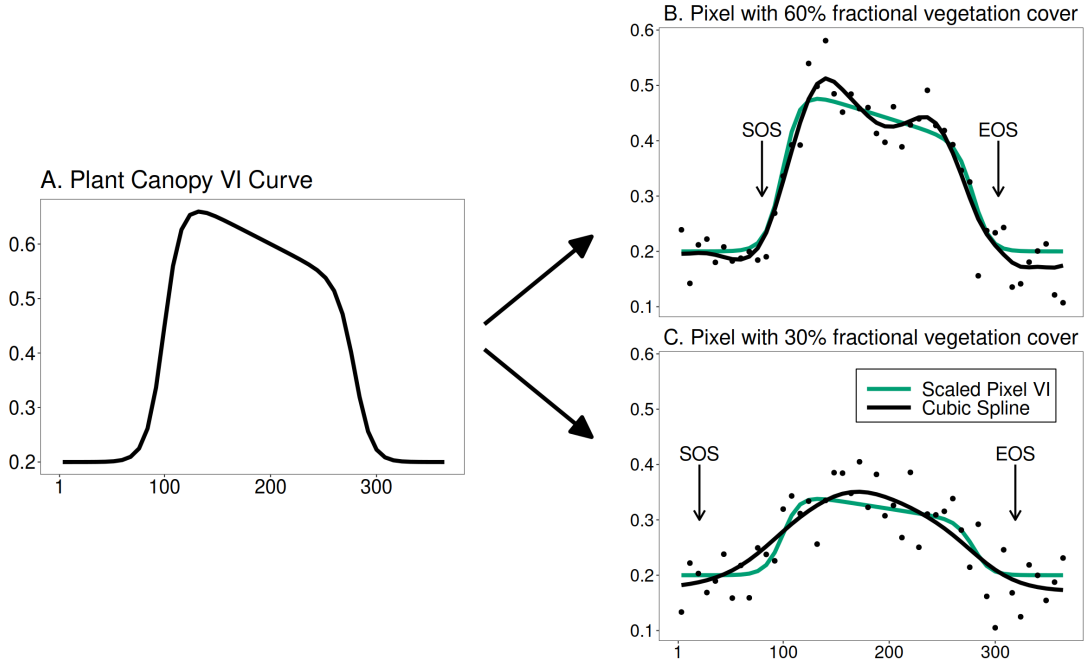


Figure 1: Conceptual diagram of simulating a VI curve with different levels of fractional vegetation cover. Panel A shows an idealized VI curve represented by a plant canopy (ie. 100% fractional vegetation cover). Panels B and C show the same curve scaled to pixels simulating 60% and 30% plant cover, respectively (green lines). The points represent the scaled curve plus VI uncertainty, with the black line representing cubic spline fit from the points. Phenological metrics (start of season, SOS, and end of season, EOS) can then be extracted from the cubic spline curve. The process is repeated with different amplitudes (ie. the curve height in panel A), plant cover values, and uncertainty size.

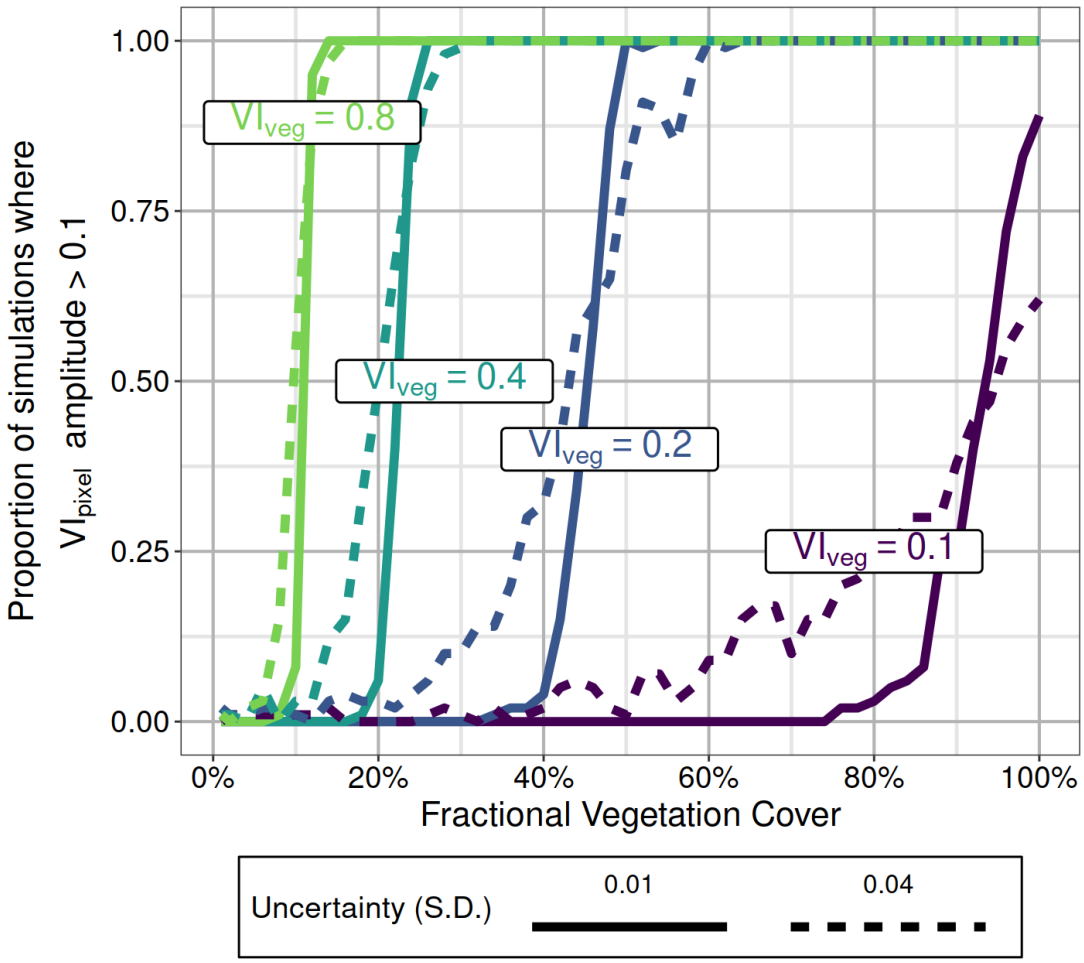


Figure 2: The proportion of simulation runs where the final $VI_{pixel}$ amplitude exceeds the 0.1 threshold. Colors indicate starting amplitudes of the pure endmember $VI_{veg}$ curve. Uncertainty is the standard deviation (SD) of the zero centered gaussian noise of the model.

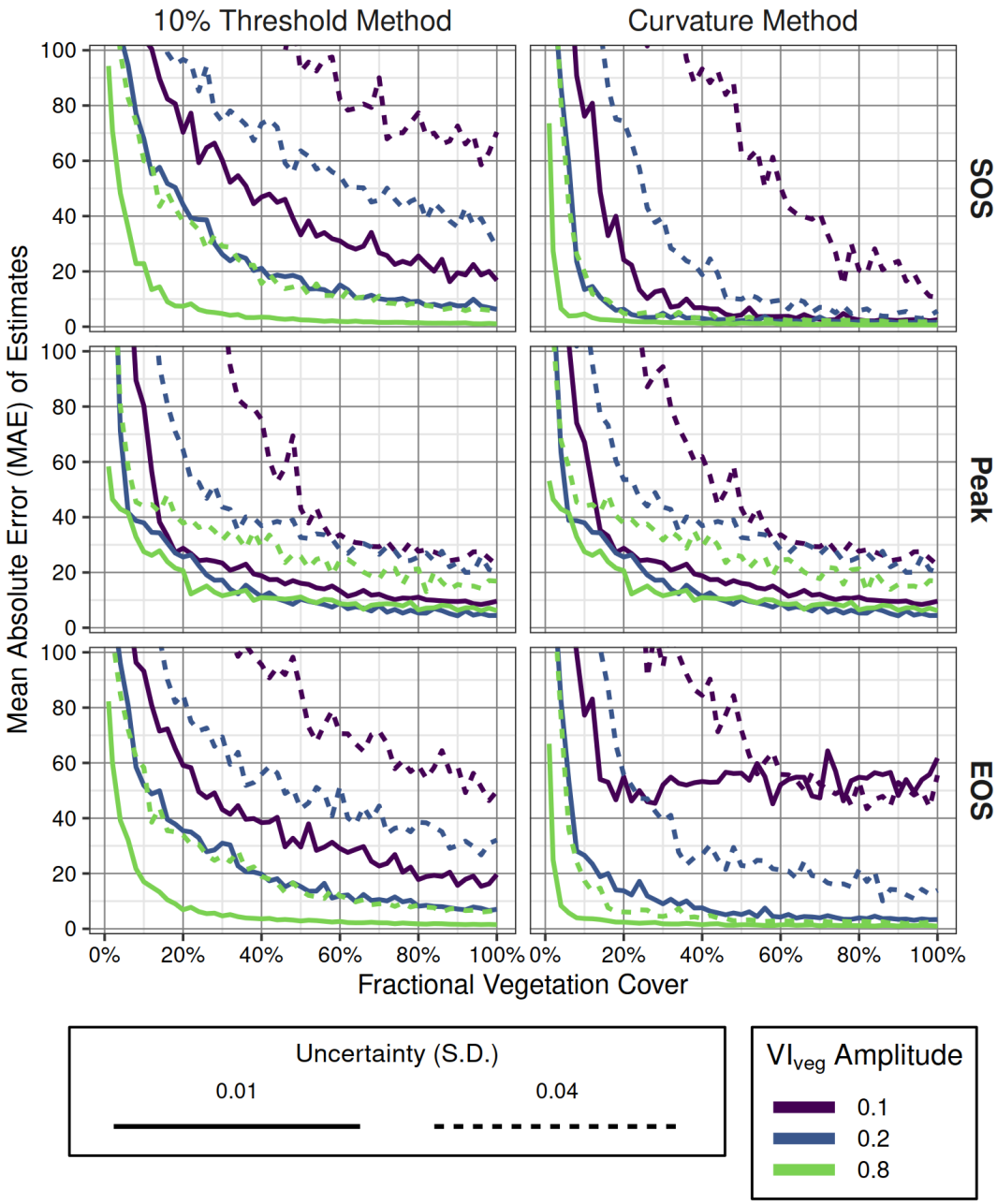


Figure 3: Mean absolute error (MAE) of three phenological metrics estimated from simulated annual vegetation index time series. Start of season (SOS), peak, and end of season (EOS). Colored lines indicate the amplitude of the endmember vegetation ($VI_{veg}$). Uncertainty is the standard deviation (SD) of the zero-centered gaussian noise of the model. Percent of maximum thresholds are those used in the SOS and EOS estimations. The $VI_{veg}$ amplitude of 0.4 is excluded for clarity.

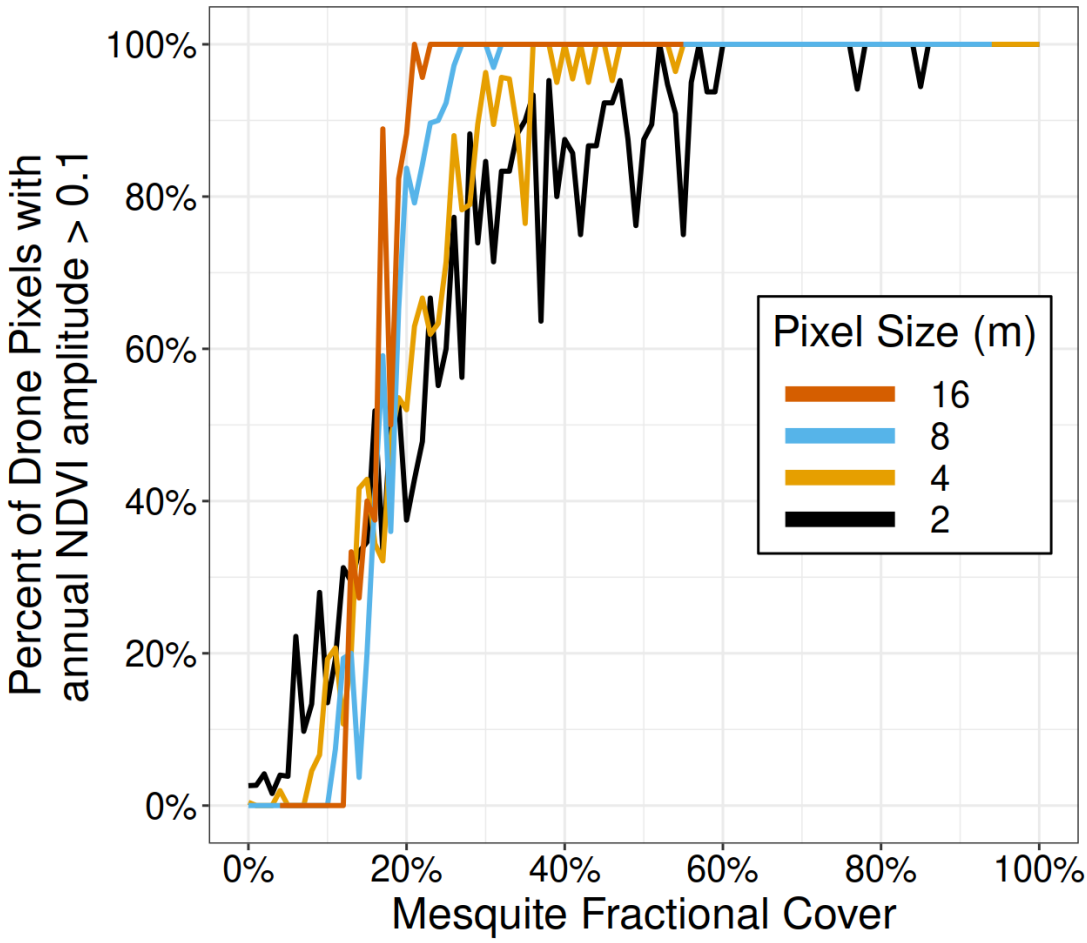


Figure 4: The proportion of pixels where the annual NDVI amplitude exceeds the 0.1 threshold. Colors reflect the simulated pixel size in meters.

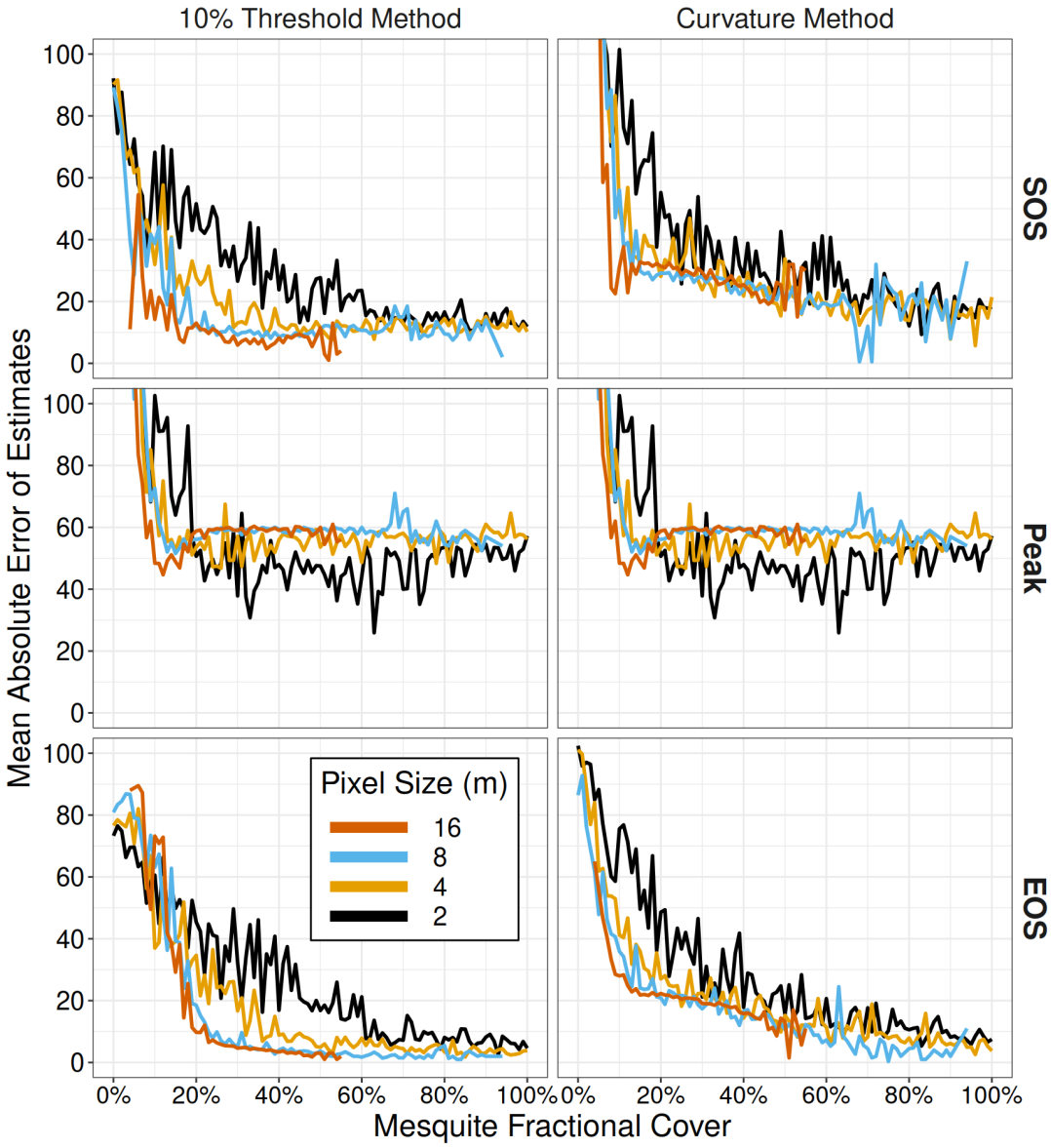


Figure 5: The mean absolute error (MAE) of phenological estimates from 12,000 simulated pixels, with sizes from 2-16m, in an annual UAV imagery timeseries. Phenological metrics are the day of year for start of season (SOS), end of season (EOS) and peak greenness (peak). True metrics were obtained from weekly in-situ observations throughout the year.

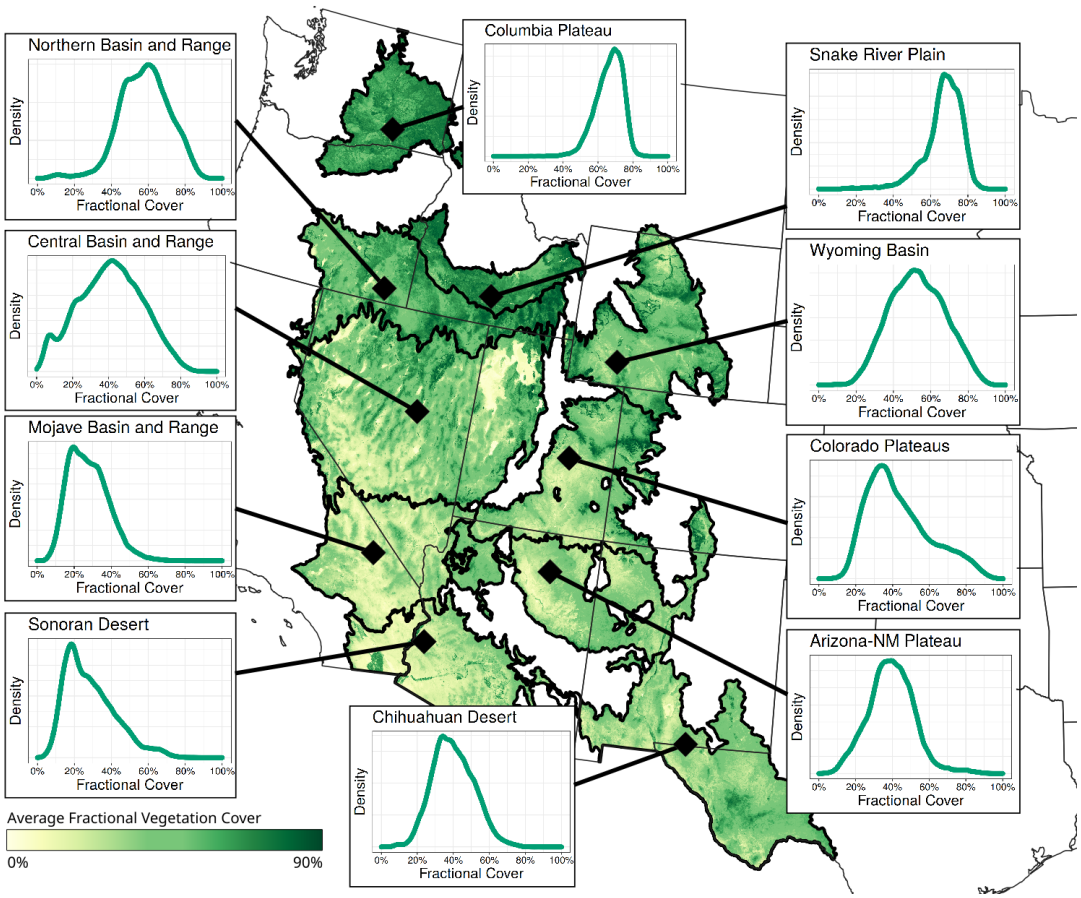


Figure 6: Average annual fractional vegetation cover across Level 3 North American Desert Ecoregions in the United States. Cover represents the average cover from 2000-2019, where the annual cover is the sum of trees, shrubs, annual and perennial forbs and grasses. Inset figures are density plots of the fractional cover for the respective ecoregion. Derived from the dataset in Allred et al. 2021 [88].

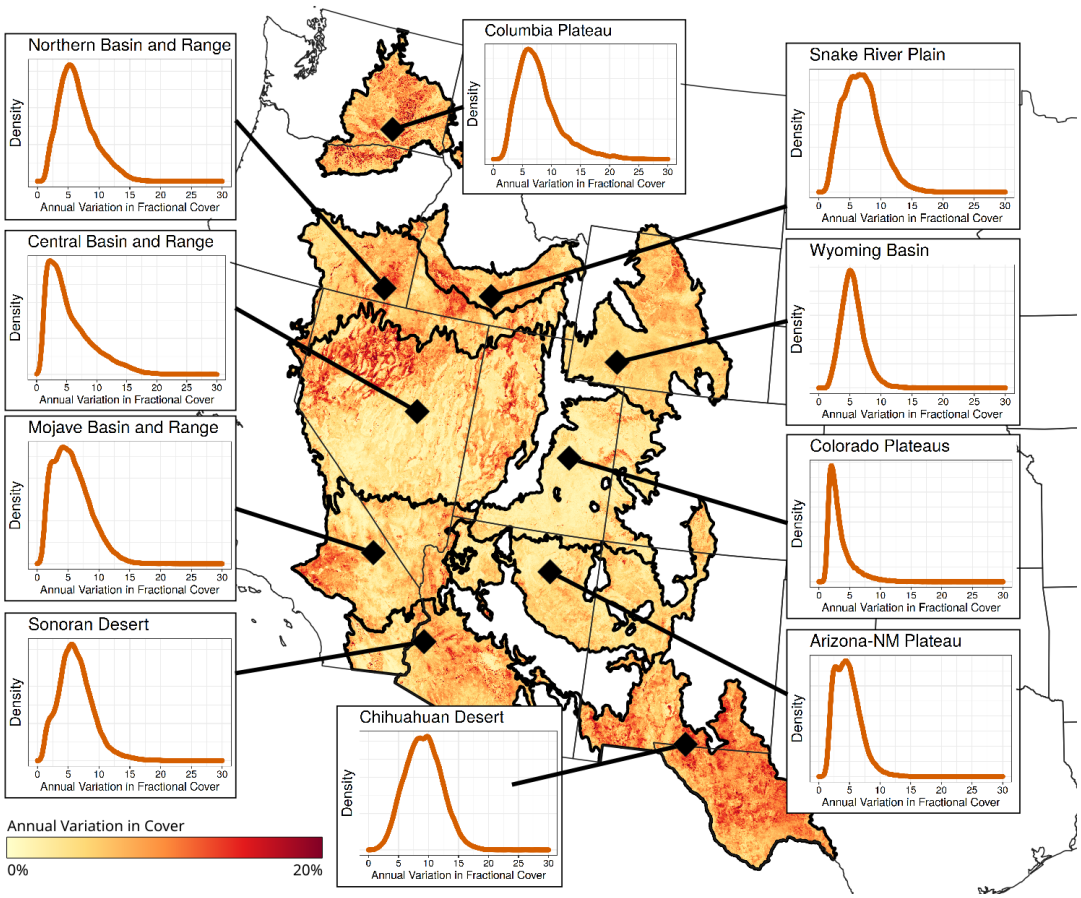


Figure 7: Variation in annual fractional vegetation cover across Level 3 North American Desert Ecoregions in the United States. Cover represents the standard deviation in cover from 2000-2019, where yearly cover is the sum of trees, shrubs, annual and perennial forbs and grasses. Inset figures are density plots of the year to year standard deviation in fractional vegetation cover for the respective ecoregion. Derived from the dataset in Allred et al. 2021 [88].

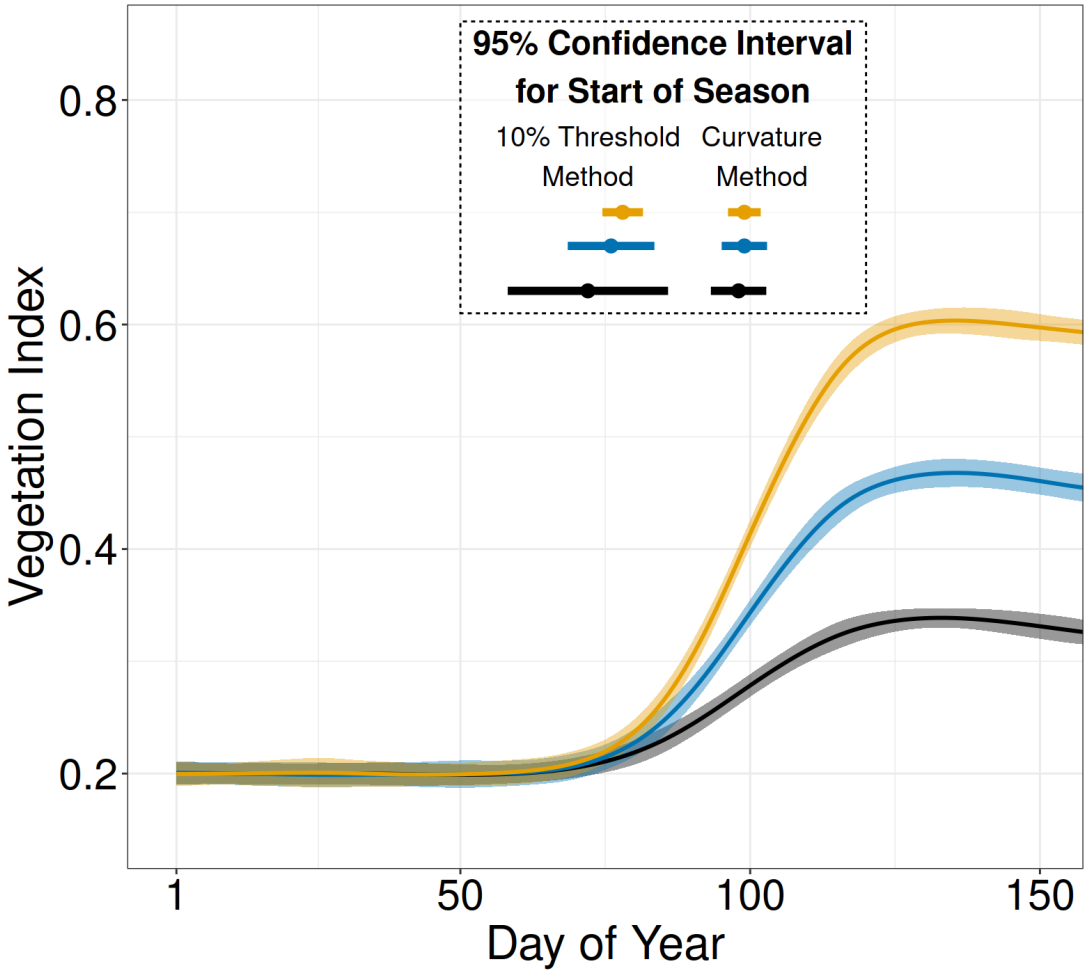


Figure 8: Three simulated VI curves with the same VI uncertainty (SD = 0.01) but different seasonal amplitude. Ribbons represent the 95% confidence interval around each VI curve as estimated from a cubic smoothing spline. Start of season estimates align with the x-axis, and are based on either a 10% of maximum threshold or the curvature method. Horizontal lines for the start of season estimates represent the mean and 95% confidence interval corresponding to the respective method and same colored VI curve, and align with the x-axis.